ELSEVIER

Catalysis Today 53 (1999) 161–176

CATALYSIS TODAY

www.elsevier.com/locate/cattod

Prediction of global reaction kinetics by solution of the Arrhenius parameterised component elementary reactions: microkinetic analysis

Kenneth C. Waugh *

Department of Chemistry, UMIST, P.O. Box 88, M60 1QD Manchester, UK

Abstract

Microkinetic analysis of heterogeneous catalytic reactions originated in the early 1970s from a program (KINPAK) that was written to predict the performance of an industrial naphta cracker. This program accepted as input a statement of elementary gas phase cracking and radical-induced hydrogen abstraction reactions, together with their Arrhenius parameters. The reactor conditions of temperature, pressure, flow rate, reactor dimensions, composition of feed, heats of formation of reactants and products, heat capacities, heat transfer coefficients, etc. were also included in the input. Mass balance equations were constructed for every component in the reaction, and the resulting matrix of non-linear equations was solved by a highly modified form of Newton–Raphson iteration [1]. Modification of this program to make it applicable to gas–solid heterogeneous catalysis was effected simply by adding a component that did not flow through the reactor — a catalyst. This paper is a review of the application of this methodology in its application to the industrially important reactions, ammonia synthesis and the water gas shift reaction.

It was first applied to the synthesis of ammonia, for which the overall potential diagram constructed from single-crystal data was well established [3]. The surprising result obtained from it was that it predicted rates of ammonia synthesis that were five orders of magnitude too low [2]. Incorporating an energy barrier to nitrogen adsorption, for which experimental evidence from catalytic data existed [13], into the potential energy surface resulted in an exact fit between prediction and experiment [2]. (Changing the original values of the pre-exponential terms from those derived from transition state theory to those obtained experimentally in single-crystal experiments improved the quality of the single-crystal data derived potential to 10% of experiment, thus highlighting the importance of the factors in the calculations [16].) Validation of the requirement for an activated adsorption has been found in the recent experimental determination by temperature programmed adsorption of the energy barrier to nitrogen adsorption on a real catalyst [20].

The program has also been applied to the water gas shift reaction over a $Cu/ZnO/Al_2O_3$ catalyst [21–23]. Here, its application demonstrated clearly the non-uniqueness of the mechanism. A previous kinetic analysis using rate expressions had claimed that it ‘proved’ that the reaction proceeded through a formate intermediate [24]. This application of KINPAK incorporated a redox mechanism, in which water oxidised the copper, producing hydrogen, while CO reduced the copper, producing CO_2. An exact fit between prediction and experiment could be obtained. This application also highlighted the interplay between the separate elementary energetics; different combinations of the activation energies of adsorption of hydrogen and of carbon dioxide to produce an adsorbed carbonate species resulted in the same overall activation energy, but totally different adsorbate compositions and totally different overall activities.

* Corresponding author. Fax: +44-161-200-4430
E-mail address: ken.waugh@umist.ac.uk (K.C. Waugh)

PII: S0920-5861(99)00114-5

The methodology imposes a strict rigour on the mechanisms that are proposed and on the limits within which elementary activation energies can be changed, since the overall potential energy surface is fixed by the heats of formation of the reactants and products.

Keywords: Global reaction simulation; Fundamental kinetics; Elementary reactions; Arrhenius parameters

1. Introduction

Microkinetic analysis in heterogeneous catalysis originated in the early 1970s from a far-sighted paper by Bush and Dyer, entitled The experimental and computational determination of complex chemical kinetics mechanisms [1]. This paper derived from a recognition within industry that, in the development of a mathematical model suitable for the design of a new process, some of the determining features of the system were often not recognised at the outset. Since reformulation and reprogramming of the model was time consuming (and costly), the need was apparent for an approach that permitted the structure of the model to be reformulated by changing the input data in the same way as the parameter values were changed. Using the examples of high temperature chlorination reactors and of hydrocarbon cracking processes, the paper described the method for altering the structure of a model without re-programming, in systems in which there were combined flow, chemical and physical state changes [1].

The computer program, which was written on the basis of the paper, accepted, therefore, as input a statement of all the elementary reactions involved, in, say, hydrocarbon cracking. These reactions were given their forward and reverse Arrhenius parameters, all of which were available in the literature. The program then constructed a matrix of mass balance equations, comprising all of the components in the reactions (in the case of heterogeneous catalysis, this included the surface and the adsorbed species) and solved these equations by Newton–Raphson iteration. A convergent solution was considered to have occurred when the sum of the squares of the rates of change of all the components is less than a pre-set very small value (usually taken to be 10^{-20}). The program then printed out the convergent values of the concentrations of all of the components of the reactions (including adsorbed species in the case of heterogeneous catalysis), which are taken to be their steady state values, obtaining under the conditions of flow rate, temperature, pressure, catalyst weight, catalyst surface area, etc., set at the beginning.

Its first application in the case of hydrocarbon cracking was typical of its subsequent use. In that case, the Arrhenius parameters of the elementary reactions involved, which had been obtained experimentally in a given temperature regime (500–700 K), were applied to a much higher temperature regime (750–1000 K). The application is one of extrapolation. Surprisingly, only minor adjustments to some of the pre-exponential terms were required to obtain a fit between prediction and experiment [1].

1.1. Microkinetic analysis applied to ammonia synthesis

The method was first applied to heterogeneous catalysis in a paper, entitled “Extrapolation of the kinetics of model ammonia synthesis catalysts to industrially relevant temperatures and pressures” [2]. Ertl and co-workers had published the complete potential energy for the synthesis of ammonia over a potassium-promoted iron catalyst (Fig. 1) [3]. This potential energy diagram was the compilation of a series of kinetic surface science experiments that measured: (i) the nitrogen sticking probabilities [4], (ii) the molecular nitrogen desorption activation energy [5], (iii) the nitrogen atom desorption activation energy [6], and (iv) the desorption activation energy of ammonia [7]. These surface science experiments were carried out at dosing pressures of $\sim 10^{-12}$ bar and temperatures of $\sim$100 K; ammonia, however, is synthesised industrially at 100 bar and 723 K. The extrapolation, therefore, is approximately 600 K and a factor of 10^{14} in pressure. The purpose of our paper was to examine the validity of this extrapolation. It was to determine whether factors not accounted for under conditions of ultra high vacuum, e.g., the possible formation of a bulk nitride under industrial conditions of high temperature and pressure (the ‘pressure gap’),

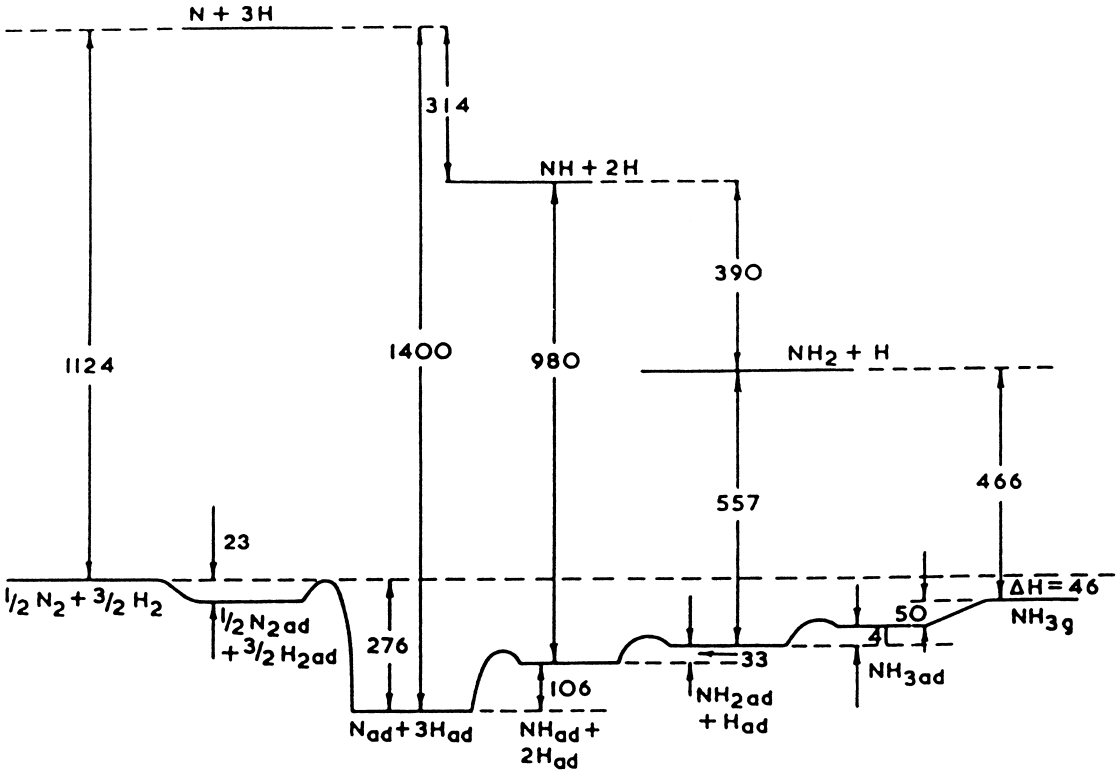

Fig. 1. Potential energy diagram for ammonia synthesis on a promoted iron catalyst.

would significantly affect the energetics of some of the elementary processes, the kinetics of which had been measured under ultra high vacuum. Evidence for pressure-induced changes in the kinetics would be found in lack of fit between ammonia synthesis rates predicted by the program and those found industrially.

1.2. Activation energies of the elementary reactions

Table 1 is the transcription of the potential energy diagram of Fig. 1 into elementary reactions. The forward and reverse activation energies of each of these elementary reactions, listed in Table 1, are taken directly from Fig. 1.

1.3. The values of the pre-exponential terms of the elementary reactions

The potential energy diagram does not provide the values of the pre-exponential terms for the reactions. The values listed in Table 1 derived from a series of sources. The desorption reaction pre-exponential terms were given the standard value of the vibrational frequency of an adsorbed species, $10^{13}\,s^{-1}$. The reaction was assumed to be taking place in a fully mixed system, and so the adsorption pre-exponential terms, which are in units of $cm^3\,mol^{-1}\,s^{-1}$, have been assigned the values of the standard collision number ($10^{13}\,cm^3\,mol^{-1}\,s^{-1}$).

Assigning values for the pre-exponential terms of the bimolecular surface reactions was more problematic. In our first paper, we used transition state theory and partition functions to calculate the value of the bimolecular surface reaction pre-exponential term for two distinct types of surface reactions: (i) a surface reaction involving immobile adsorbates producing an immobile transition state, and (ii) a surface reaction involving mobile adsorbates producing a mobile transition state [2].

The rate/$cm^{-2}\,mol\,s^{-1}$ of the bimolecular surface reaction

Table 1
Elementary reactions of the low coverage ammonia potential energy surface

Reaction no.	Forward Arrhenius parameters		Stoichiometry of elementary reactions	Reverse Arrhenius parameters	
	$\log_{10}$ (A/units)	E/J mol^{-1}		$\log_{10}$ (A/units)	E/J mol^{-1}
1	13.00	00 000	$N_2 + FE \Leftrightarrow N_2A$	13.0	46 000
2	21.00	46 000	$N_2A + FE \Leftrightarrow NA + NA$	21.0	225 804
3	13.00	0 000	$H_2 + FE \Leftrightarrow H_2A$	13.0	0 000
4	21.00	0 000	$H_2A + FE \Leftrightarrow HA + HA$	21.0	108 732
5	20.8	12 5910	$HA + NA \Leftrightarrow NHA + FE$	21.0	20 910
6	20.8	53 910	$HA + NHA \Leftrightarrow NH_2A + FE$	21.0	20 910
7	20.7	62 730	$HA + NH_2A \Leftrightarrow NH_3A + FE$	21.0	20 910
8	13.0	50 184	$NH_3A \Leftrightarrow NH_3 + FE$	13.0	0 000

$$A_{(a)} + B_{(a)} \rightleftharpoons AB^{\#}_{(a)} \quad (1)$$

where the subscript (a) denotes adsorbed species and the superscript # denotes the transition state, is given by

$$\text{Rate/mol cm}^{-2}\,\text{s}^{-1} = N\frac{kT}{h}\frac{q_{AB^{\#}}}{q_A q_B}\rho_A\rho_B e^{-E^{\#}/RT} \quad (2)$$

where N is Avogadro's number, k is Boltzmann's constant, T is the absolute temperature, h is Planck's constant, the q's are the molecular partition functions, the ρ's are surface densities of the reactants in units of mol cm^{-2}, $E^{\#}$ is the activation energy for the formation of the adsorbed transition state and R is the gas constant.

Factoring the partition functions into their translational, vibrational and rotational components, Eq. (2) became

$$\text{Rate/mol cm}^{-2}\,\text{s}^{-1} = N\frac{kT}{h}\frac{q_{AB^{\#}_{trans}} q_{AB^{\#}_{vib}} q_{AB^{\#}_{rot}}}{q^2_{A_{trans}} q_{A_{rot}} q_{A_{vib}} q^2_{B_{trans}} q_{B_{vib}} q_{B_{rot}}}\rho_A\rho_B e^{-E^{\#}/RT} \quad (3)$$

For immobile adsorbates and transition state, the translational energy was zero and the translational partition function, which is given by

$$q_{itrans} = \sum g_i e^{-\varepsilon_{itrans}/kT}$$

where ε_i is the energy of the ith state and g_i is its degeneracy, reduces to the degeneracy, g, which is the number of adsorption sites per square centimetre, Ns, (10^{15} sites per square centimetre).

Since the vibrational and rotational partition functions of the adsorbates and the transition state roughly cancel the surface bimolecular pre-exponential term for immobile adsorbates producing an immobile transition state is

$$\text{A/cm}^2\,\text{mol}^{-1}\,\text{s}^{-1} = \frac{N}{N_s}\frac{kT}{h}$$

$$\approx 10^{21}$$

Using similar arguments, for mobile adsorbates producing a mobile transition state, the surface bimolecular pre-exponential term is

$$\text{A/cm}^2\,\text{mol}^{-1}\,\text{s}^{-1} = N\frac{kT}{h}\frac{1}{q^2_{A_{trans}}}$$

where $q^2_{A_{trans}} = \frac{2\pi mkT}{h^2} \approx 10^{16}$, and so A/cm^2 mol^{-1} s^{-1} $\approx 10^{21}$.

For the bimolecular surface reaction between one mobile and one immobile adsorbate producing an immobile transition state, the pre-exponential term is [8,9]

$$\text{A/cm}^2\ \text{mol}^{-1}\ \text{s}^{-1} = N\frac{kT}{h}\frac{1}{q^2_{A_{trans}}}$$

$\approx 10^{21}$ and for one mobile and one immobile adsorbate producing a mobile intermediate the A-factor is

$$\text{A/cm}^2\ \text{mol}^{-1}\ \text{s}^{-1} = N\frac{kT}{h}\frac{q^2_{AB^{\#}_{trans}}}{Nsq^2_{A_{trans}}}$$

$$= \frac{N}{Ns}\frac{kT}{h}$$

$$\approx 10^{21}$$

Therefore, for all types of bimolecular surface reactions, the pre-exponential term has a value of 10^{21} cm^2 mol^{-1} s^{-1}. Minor variations from this to 20.8, and 20.7 for the forward reactions, 5, 6 and 7 are included so that the program accurately predicts equilibrium.

The equations listed in Table 1 were solved in the temperature range 673–773 K at 107 atm for a gas hourly space velocity of 16 000 h^{-1} for a catalyst surface area of 10 m^{-2} g^{-1}. The outcome, listed in Table 2, shows that the predicted exit ammonia concentrations were $\sim 10^5$ times too low, the cause being that the nitrogen atom well depth was too low, producing a self-poisoning, totally nitrided surface [2]. The rate determining step predicted by this potential was the hydrogenation of the adsorbed nitrogen atom, and not dissociation of the molecular nitrogen precursor state which Ertl had claimed to be rate determining [4].

1.4. Alternative models for ammonia synthesis

Four other forms of potential were examined in our original paper [2]. These were (i) a high coverage potential, (ii) a low coverage, low nitrogen sticking probability potential, (iii) a high coverage, low nitrogen sticking probability potential, and (iv) a high coverage activated nitrogen adsorption potential.

1.5. High coverage potential energy surface

The only elementary reaction in the complete ammonia potential energy diagram that showed any dependence on coverage, was hydrogen desorption [10]. The high coverage hydrogen desorption activation energy is 63 kJ mol^{-1}. This raised the nitrogen atom/hydrogen atom well depth from 276 kJ mol^{-1} to 207 kJ mol^{-1} — this energy difference of 69 kJ mol^{-1} being transferred to the activation energy of the first hydrogenation step, which was lowered from 106 kJ mol^{-1} to 37 kJ mol^{-1}. The outcome was virtually identical to that produced by the low coverage potential (Table 2). The nitrogen atom well depth was still too great and the prediction was for a totally nitrided surface with a rate of ammonia synthesis 10^5 times smaller than experiment.

1.6. Low coverage, low nitrogen sticking probability potential energy surface

It was pointed out that equating the rate of nitrogen adsorption with the standard collision number would overestimate the nitrogen atom coverage, since it had been shown experimentally that the nitrogen sticking probability was $\sim 10^{-7}$ [11]. Consequently, the values of the pre-exponential terms for nitrogen dissociative adsorption (reaction 2, Table 1) and for nitrogen atom recombination (the reverse reaction 2, Table 1) were lowered by factors of 10^7. The potential energy diagram shown in Fig. 1 was unchanged. The surface coverages predicted by this model were of a much lowered nitrogen atom coverage (1% of a monolayer), but of a surface that was nearly totally hydrided (∼96%). The predicted rates of ammonia synthesis, therefore, were still 10^4 times lower than experiment.

1.7. High coverage, low nitrogen sticking probability potential energy surface

It seemed self-evident that combining the lowered energy barrier for the first nitrogen atom hydrogenation step of the high coverage potential with the lowered nitrogen atom coverage of low nitrogen atom sticking probability would lead to a model that would accurately predict experimentally observed ammonia synthesis rates. Surprisingly, this was not the case. The predicted rates of ammonia synthesis were 10^4 times too small, even though the nitrogen atom coverage is now reduced to 92% of a monolayer. The low hydrogen atom coverage of 6% of a monolayer appeared to inhibit the rate of ammonia synthesis (the experimentally determined nitrogen atom/hydrogen atom coverage of a commercial ammonia synthesis catalyst, which had been producing ammonia at 1 bar from a 3 : 1 hydrogen/nitrogen mixture, was 75% of a monolayer of hydrogen atoms and 25% of a monolayer of nitrogen atoms [12]).

1.8. High coverage, activated nitrogen adsorption potential energy surface

It was suggested [11] that a potential should be explored, in which the adsorption of nitrogen into the atomic state was activated having an energy barrier

Table 2
Consequences of the low coverage ammonia potential energy surface

Temp (°C)	Flow rate ($cm^3\,s^{-1}$)	Pressure (atm)	NH_3 (%)			Predicted surface coverage (% free iron)					
			Predicted	Experimental	Equilibrium	N_2A	NA	HA	NHA	NH_2A	NH_3A
400	0.0275 (GHSV = 16 000 h^{-1})	107	8.4×10^{-6}	–	~25.4	5×10^{-5}	99.99	0.01	8×10^{-5}	2×10^{-5}	4×10^{-11}
400	1.0×10^{-20}	100	25.5	25.4	25.4	1×10^{-5}	99.99	5×10^{-3}	3×10^{-4}	2×10^{-4}	3×10^{-5}
425	0.0275	107	2.8×10^{-5}	–	~22.0	7×10^{-5}	99.99	7×10^{-3}	1×10^{-4}	3×10^{-5}	2×10^{-10}
450	0.0275 (GHSV = 16 000 h^{-1})	107	8.7×10^{-5}	13.2	~16.4	9×10^{-5}	99.99	0.01	2×10^{-4}	4×10^{-5}	6×10^{-10}
450	0.04125 (GHSV = 24 000 h^{-1})	107	5.8×10^{-5}	12.5	~16.4	9×10^{-5}	99.99	0.01	2×10^{-4}	4×10^{-5}	4×10^{-10}
450	1.0×10^{-20}	100	16.8	16.4	16.4	3×10^{-5}	99.99	0.01	5×10^{-4}	3×10^{-4}	4×10^{-5}
475	0.0275	107	2.5×10^{-4}	–	~14.0	1×10^{-4}	99.986	0.014	3×10^{-4}	6×10^{-5}	2×10^{-9}
500	0.0275	107	6.6×10^{-4}	–	~11.0	2×10^{-4}	99.98	0.019	4×10^{-4}	8×10^{-5}	7×10^{-9}
500	1.0×10^{-20}	100	11.0	10.5	10.5	6×10^{-5}	99.98	0.019	8×10^{-4}	4×10^{-4}	5×10^{-5}

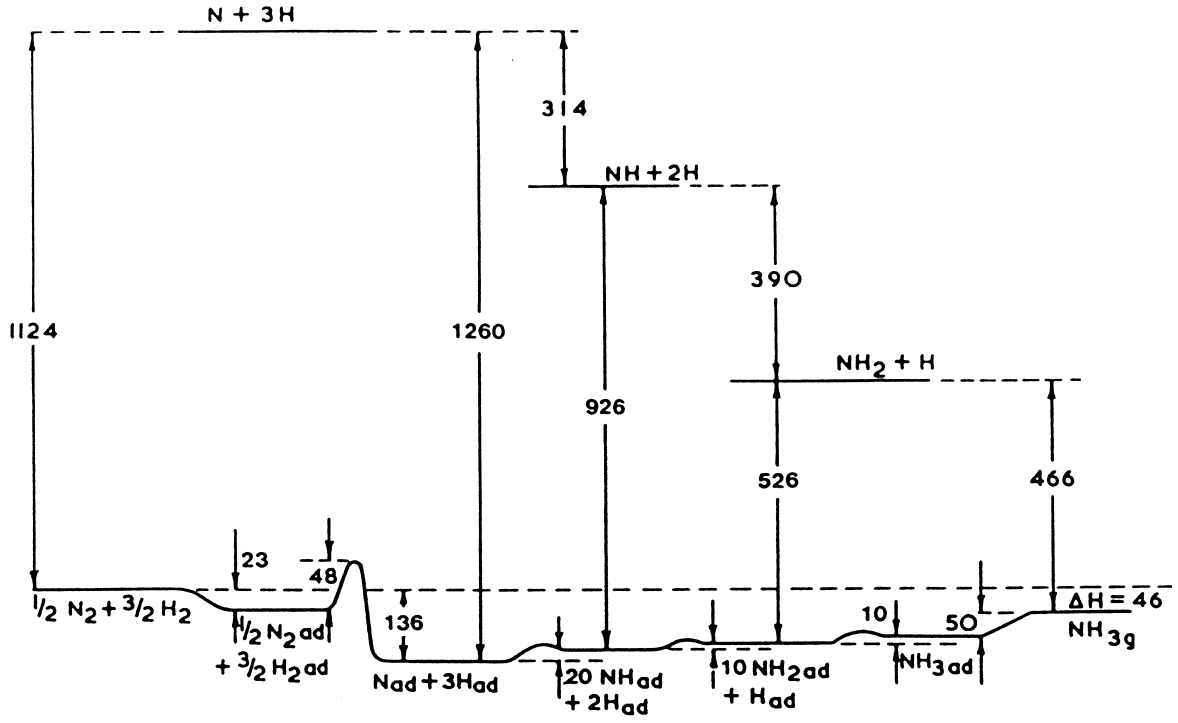

Fig. 2. Potential energy diagram for ammonia synthesis on a promoted iron catalyst with activated adsorption.

similar to that found by Scholten and co-workers for the adsorption of nitrogen on an alumina-supported iron catalyst [13]. Scholten and co-workers had reported a value of 96 kJ mol^{-1} for the high coverage activation energy for the dissociative adsorption of nitrogen. They also reported an activation energy of 134 kJ mol^{-1} for the recombinative desorption of the atomic nitrogen [13]. These were introduced into a potential energy diagram, in which the value of the heat of adsorption of molecular nitrogen of 46 kJ mol^{-1} was retained and in which the high coverage value of the hydrogen atom desorption activation energy (E_{d-4} = 63 kJ mol^{-1}) was also used. The overall potential energy diagram that resulted from this is shown in Fig. 2. The striking feature of this diagram is the shallowness of nitrogen–hydrogen atom well (136 kJ mol^{-1}), so that only 90 kJ mol^{-1} was required to move from that point to gas phase ammonia.

The elementary activation energies resulting from this potential energy diagram were coupled with the pre-exponential terms listed in Table 1 and the matrix of non-linear equations was solved in KINPAK. Its prediction of the exit ammonia concentrations and of the nitrogen and hydrogen atom coverage of the catalyst at 107 bar and between 673 and 773 K are shown in Table 3.

The predicted exit ammonia concentrations were within 10% of those found experimentally. The predicted overall activation energy, calculated from the model by using extremely short contact times, was 117 kJ mol^{-1}, a value which is somewhat higher than that (81 kJ mol^{-1}) obtained by Somorjai and co-workers on Fe(111) at 20 atm in the temperature range 673 to 823 K [14]. It was emphasised at the time that, although the model was remarkably good (remembering that no attempt had been made to fit the data), there was no experimental evidence that, in a doubly promoted industrial catalyst (Fe/K/Al_2O_3), an energy barrier existed to dissociative nitrogen adsorption [2].

Our original paper provoked strong criticism from Stoltze and Norskov [15]. They reported an exact fit

Table 3
Consequences of the high coverage ammonia potential energy surface with activated adsorption of nitrogen from the molecular precursor state

Temperature (°C)	Flow rate ($cm^3\,s^{-1}$)	Pressure (atm)	NH_3 (%)			Predicted surface coverage (% free iron)						
			Predicted	Experimental	Equilibrium	N_2A	NA	NHA	NH_2A	HA	Fe	NH_3A
400	0.0275 (GHSV = 16 000 h^{-1})	107	12.8	–	~25.4	5.1	40.1	7.1	6.8	31.3	3.2	6.3
400	1.0×10^{-20}	100	25.56	25.4	25.4	2.2	57.4	9.0	7.8	15.3	1.8	6.5
425	0.0275	107	14.28	–	~22.0	3.7	48.7	7.7	6.4	25.3	3.3	5.0
450	0.0275 (GHSV = 16 000 h^{-1})	107	14.22	13.2	~16.4	2.9	54.1	7.9	5.6	22.1	3.5	3.8
450	0.04125 (GHSV = 24 000 h^{-1})	107	13.18	12.5	~16.4	3.1	52.5	7.7	5.5	23.7	3.7	3.8
450	1.0×10^{-20}	100	16.8	16.4	16.4	2.2	59.3	8.2	5.8	18.0	3.0	3.6
475	0.0275	107	12.9	–	~14.0	2.5	57.0	7.7	4.8	21.0	4.0	2.9
500	0.0275	107	11.06	–	11.0	2.3	58.3	7.4	4.1	21.0	4.7	2.2
500	1.0×10^{-20}	100	11.0	10.5	10.5	2.1	59.6	7.3	3.9	20.2	4.7	2.0

between the potential energy diagram published by Ertl and experiment over a pressure range of 1 to 300 atm [15]. The form of the microkinetic analysis used by them for these calculations, however, differed considerably from ours. They assumed that the dissociation of the molecular nitrogen precursor was rate determining and that all of the other reactions were at equilibrium. The equilibrium constants for all of the elementary reactions were obtained by calculation, using the partition functions.

An important difference between their paper [15] and ours [2] lay in their lowering of the activation for nitrogen atom recombinative desorption form Ertl's value of 213 kJ mol^{-1} to 161 kJ mol^{-1}. Their justification for this reduction in the nitrogen atom desorption energy barrier was that, since the sticking probability was anomalously low by a factor of 10^6, the desorption pre-exponential should also be reduced by the same amount. In order that the model accurately reproduced Ertl's temperature programmed desorption peak maximum temperature of 870 K [6] with this new pre-exponential value of $10^7\,s^{-1}$, the desorption activation energy was reduced to 161 kJ mol^{-1}. Stoltze and Norskov found this to be persuasive agreement for their method [15]. It raised the nitrogen–hydrogen atom energy minimum from –276 kJ mol^{-1} to 224 kJ mol^{-1}. However, the calculation was no longer being conducted on Ertl's potential energy surface.

1.9. The importance of the values of the pre-exponential terms

In our second paper on the subject, we refined three of the pre-exponential terms of our earlier paper to accord with the published values [16]. The value of the standard collision number (A_1, Table 1) was lowered from 10^{13} to 10^{11} $cm^3\,mol^{-1}\,s^{-1}$ to reflect Ertl's sticking probability of 10^{-2} for the molecular state [5,17]. The pre-exponential term for the desorption of the molecular precursor state was lowered from 10^{13} to $10^{10}\,s^{-1}$ — the value Ertl obtained by fitting the measured heat of adsorption of 46 kJ mol^{-1} to the desorption peak maximum of 210 K. Finally, the value of the pre-exponential for the dissociation of the molecular precursor state was set at 10^{15}, which was lowered from 10^{21} $cm^2\,mol^{-1}\,s^{-1}$ to reflect the measured nitrogen atom sticking probability of 10^{-6} [5,17]. The potential energy diagram used was Ertl's original low coverage surface, with the minor modification of the inclusion of intermediate value of the hydrogen atom desorption activation energy of 92 kJ mol^{-1}, consistent with our early predictions of a low hydrogen atom coverage [2].

These modifications produced the surprising result of a predicted exit ammonia yield at 720 K, 107 atm and 16 000 GHSV of 3.0%, which was a factor of 10^5 times higher than obtained previously using the same potential energy surface, but different values of

the pre-exponential terms [2]. This value, though, was still smaller than the experimental one of 13.2% [18]. The surface coverage (in monolayers) of the catalyst predicted by this model was $H_{(a)}$, 12.1%; $N_{2(a)}$, 15%; $N_{(a)}$, 84.4%; and $NH_{(a)}$, 1.9%. (Stoltze and Norskov chose to ignore terms involving the molecular nitrogen precursor state on the assumption that they would be negligibly small [15]. These calculations question the validity of this assumption.)

Changing the potential energy surface to include Stoltze and Norskov's lowered nitrogen atom desorption activation energy of 161 kJ mol^{-1}, while maintaining the refined values of the pre-exponential terms, produced a model that predicted exit ammonia concentrations of 5.4% at 723 K, 107 bar and 16 000 GHSV. This is not the exact fit claimed by Stoltze and Norskov [15].

Our second paper also explored the self-consistency of both models (ours and Stoltze and Norskov's) in terms of their prediction of the nitrogen atom desorption line shape. Whereas Stoltze and Norskov had calculated the desorption activation energy of 161 kJ mol^{-1} to replicate the nitrogen atom desorption peak maximum temperature of 870 K when combined with a pre-exponential term of 10^7 s^{-1}, when the total desorption process involving the molecular nitrogen precursor state was included, the predicted desorption peak maximum temperature was now 85 K lower than the experimental value and the predicted peak width (full width at half maximum) was 120 K compared with an experimental value of 85 K. Our model also predicted a peak maximum temperature 85 K too low, but with a peak width (FWHM) of 85 K — identical to experiment.

Our final paper on the subject of the prediction of ammonia synthesis rates examined the use of the method in respect of the reaction structure sensitivity and of the effect of the promoter [19]. Using Ertl's published single-crystal kinetics, we showed that the published kinetics did not predict that promotion would equalise the activity on all three low index faces as had been found experimentally — structure sensitivity persisted with the activities of the potassium promoted Fe(111), Fe(100) and Fe(110), being in the ratio of 41 : 15 : 1.

Use of the method of microkinetic analysis gained what might be considered to be its ultimate validation in the recent discovery by the novel technique of temperature programmed adsorption, of an activation energy for nitrogen atom adsorption on a doubly promoted ($Fe/K/Al_2O_3$) ammonia synthesis catalyst [20], in accord with the prediction of our first paper [2].

1.10. The copper catalysed forward and reverse shift reaction

A second series of paper [21–23] examined the application of the method of microkinetic analysis to the forward and reverse water gas shift reaction. The temperature dependence of the rates of reaction of the reverse water gas shift reaction had been determined experimentally on polycrystalline copper [21] and it was these data that were used for comparison with the predicted rates.

The first two papers were essentially illustrative [21,22]. Herwijen and De Jong had claimed that a kinetic analysis of the shift reaction proved that the reaction proceeded through a formate intermediate [24]. We had shown that carbon dioxide decomposed on polycrystalline copper [25] and that it did so through the mediation of a weakly held molecular precursor state [26]. We had also shown that water decomposed on copper with an overall activation energy of 27 kJ mol^{-1} [27].

It was possible, therefore, to write the potential energy diagrams for the complex reactions

$$CO + O_{(a)} \rightleftharpoons CO_2 + Cu \qquad (A)$$

$$H_2O + Cu \rightleftharpoons H_2 + O_{(a)} \qquad (B)$$

These are shown in Figs. 3 and 4. Their combination constitutes a statement of the forward and reverse shift reactions employing a redox mechanism. A re-statement of the forward and reverse shift reaction, in terms of the elementary reactions which constitute the reactions A and B, is given in Table 4. This table also lists the values of the pre-exponential terms of each of these elementary reactions.

Although this model gave an exact fit to the experimentally obtained temperature dependence of the rates of the RWS reaction, it was well understood that the model was deficient in several respects. The first recognised deficiency was that the activation energy for the adsorption of hydrogen (as atoms) on Cu was set to zero. This was the accepted view at the time of writing the model [21]. However, it was subsequently

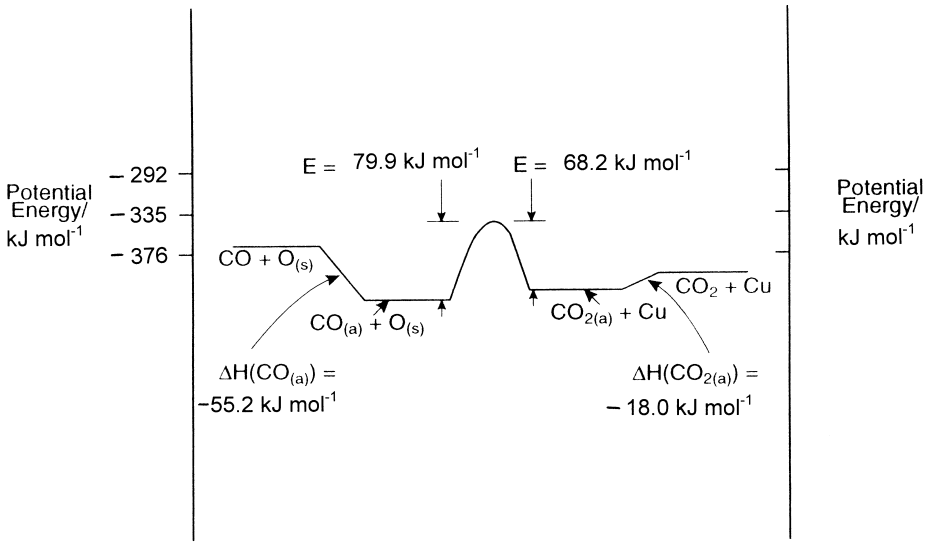

Fig. 3. Potential energy diagram for the reaction $CO + O_{(s)} \rightleftharpoons CO_2 + Cu$.

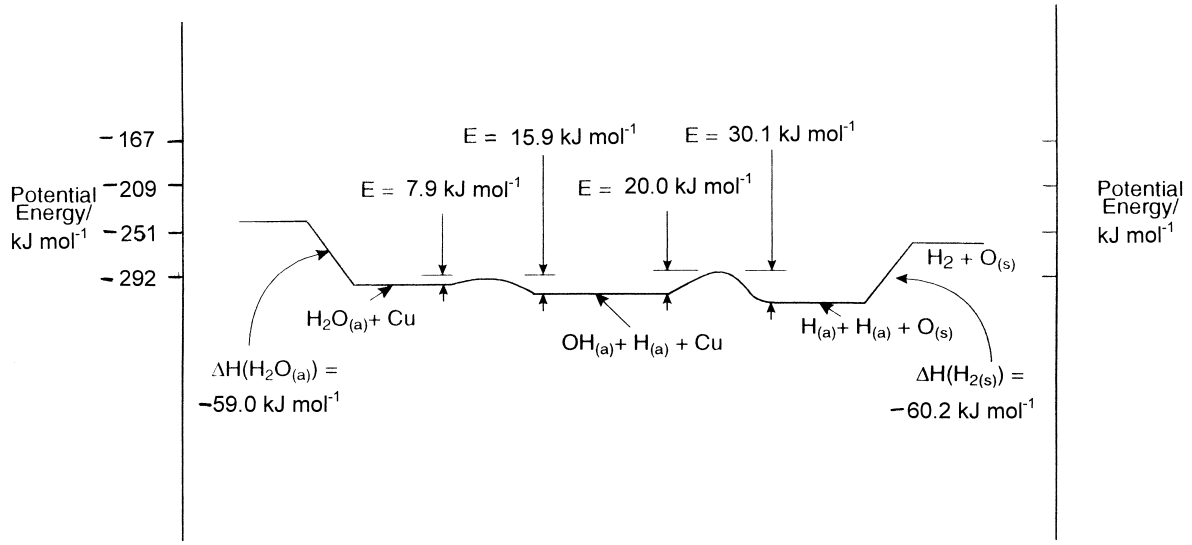

Fig. 4. Potential energy diagram for the reaction $H_2O + Cu \rightleftharpoons H_2 + O_{(s)}$.

shown in a number of papers that the chemisorption of hydrogen on Cu was activated [28–32]. The consequence of this omission on the results produced by the model, however, were predicted to be an overestimate of the hydrogen coverage.

A second deficiency related to the formation of a surface carbonate on the copper. We had shown that the initial interaction of carbon dioxide with clean copper is dissociative, producing carbon monoxide and a surface oxidised copper [25]. Subsequent adsorption of carbon dioxide onto this surface oxidised copper produced a surface carbonate species [33]. The existence of the surface carbonate will block part of the copper and so reduce the overall rate of reaction. This was not considered in our shift reaction model [22] although the exact value of its energy barrier to adsorption is in doubt with activation energies in the range 40 to 60 kJ mol^{-1} being reported [28–32].

Table 4
Elementary reactions of the forward and reverse shift reaction

Reaction no.	Forward Arrhenius parameters		Stoichiometry of elementary reactions	Reverse Arrhenius parameters	
	$\log_{10}$ (A/units)	E/J mol^{-1}		$\log_{10}$ (A/units)	E/J mol^{-1}
9	13	0	$CO_2 + Cu \Leftrightarrow CO_{2(a)}$	13	18 000
10	21	68 000	$CO_{2(a)} + Cu_{(a)} \Leftrightarrow CO_{(a)} + O_{(s)}$	21	80 000
11	13	55 000	$CO_{(a)} \Leftrightarrow CO + Cu$	13	0
12	13	0	$H_2 + Cu \Leftrightarrow H_{2(a)}$	13	0
13	21	0	$H_{2(a)} + Cu \Leftrightarrow H_{(a)} + H_{(a)}$	21	60 000
14	21	30 000	$H_{(a)} + O_{(s)} \Leftrightarrow OH_{(a)} + Cu$	21	20 000
15	21	16 000	$H_{(a)} + OH_{(a)} \Leftrightarrow H_2O_{(a)} + Cu$	21	8 000
16	13	59 000	$H_2O_{(a)} \Leftrightarrow H_2O + Cu$	13	0

The extent of blocking of the copper surface by the adsorbed carbonate was mitigated as a consequence of its being hydrogenated to form a formate species (also not allowed for), which, on further hydrogenation, produced methanol [33]. This reaction sequence was also missing from the model, so that not only was the standing concentration of carbonate omitted from the model predictions, so too were the surface coverages of formate and methoxy species together with predictions of gas phase methanol concentrations.

A final deficiency in the model related to the detailed kinetics of the adsorption and decomposition of carbon dioxide to carbon monoxide and an adsorbed oxygen atom. Experimentally, we had shown that the decomposition of carbon dioxide on Cu is precursor state mediated, having an activation energy of 12 kJ mol^{-1} for the decomposition of the weakly held precursor state CO_2 ($CO_{2(a)}$), which is less than the heat of adsorption of the weakly held precursor state by 4 kJ mol^{-1} [26]. However, the model (Table 4 and Fig. 3) showed an activation energy for the decomposition of the weakly held precursor state of 68 kJ mol^{-1}. This value of 68 kJ mol^{-1}, required by the combination of the kinetics and thermodynamics involved in the reverse reaction A

$$CO_{2(a)} + Cu \rightleftharpoons CO_{(a)} + O_{(a)} \qquad (A)$$

in the model was virtually identical to the value of 70 kJ mol^{-1} obtained by Campbell and co-workers for CO_2 decomposition on Cu(110) [34] and was consistent with our determination of an activation energy of approximately this value for the decomposition of CO_2 on the shift catalyst in the temperature range 300 to 470 K [35].

The paper addressed two of these omissions: activated adsorption of hydrogen on copper (for which the potential energy diagram is shown in Fig. 5) and the formation of a carbonate species on the copper surface.

1.11. Activated hydrogen adsorption

Examination of the surface coverages predicted by the activated hydrogen adsorption model (Table 5) was particularly helpful in revealing the major difference produced by including an energy barrier to the dissociation of $H_{2(a)}$. The hydrogen atom coverage dropped from 90 to 7%, and the amount of free copper surface increased from 40 to 70%. Qualitatively this was expected; the extent, however, was surprising. At low temperatures (396–324 K), the predicted hydrogen atom coverage increases from 6.8 to 7.04% of a monolayer, showing it to be kinetically controlled in this regime.

Curiously, in spite of the hydrogen atom coverage being reduced by a factor of 10 and in spite of the detailed kinetics of reaction (A) remaining unchanged, the rates of reverse shift reaction predicted by this model are higher at all temperatures than those predicted by the non-activated hydrogen adsorption model. The difference derives from the amount of free copper predicted by the two models. The larger amount of free copper (40–70% of a monolayer) predicted by the activated hydrogen adsorption allows for a greater degree of CO_2 adsorption and decomposition and hence the higher overall rates.

Topsoe and co-workers have found a maximum H : Cu ratio on dosing hydrogen alone on to copper of 0.4 at a dosing temperature of 248 K [36]. H : Cu

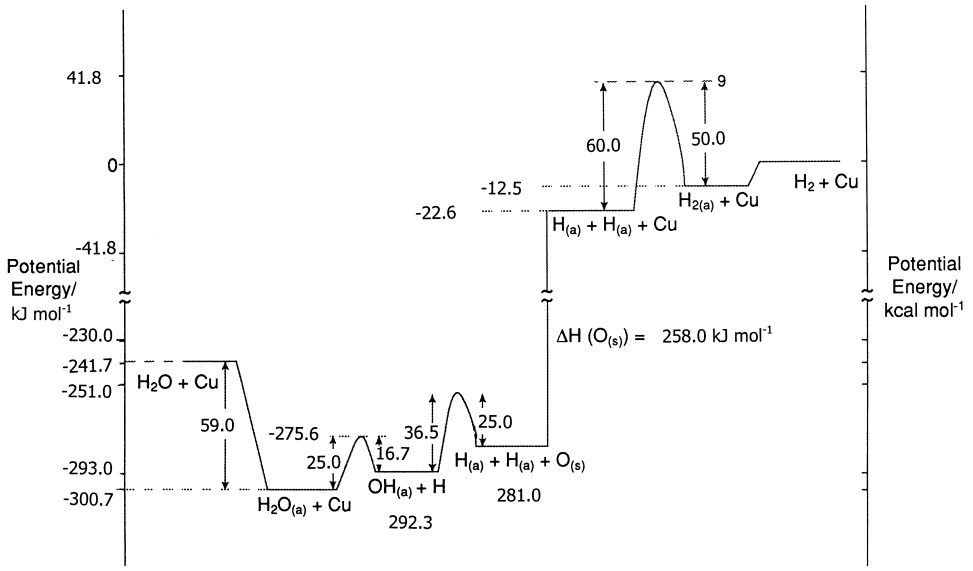

Fig. 5. Potential energy diagram for the reaction $H_2O + Cu \rightleftharpoons H_2 + O_{(s)}$ with activated H_2 adsorption.

Table 5
The overall activation energies kJ mol^{-1} for the reverse shift reaction predicted by changing both the activation energies for CO_2 and H_2 adsorption

Energy barrier to H_2 dissociative adsorption (kJ mol^{-1})	Energy barrier to CO_2 adsorption forming adsorbed carbonate (kJ mol^{-1})			
	0	21	42	63
0	91.6	86.5	97.0	97.0
8.4	89.9	108.3	110.4	109.6
16.8	88.2	86.6	88.2	67.8
25.0	87.8	66.5	25.0	43.9
33.5	87.7	64.4	26.4	25.5
41.8	87.9	64.0	22.2	18.8
50.2	87.9	63.6	19.2	18.4

ratios of roughly this value could be obtained by ranging the activation energy to hydrogen adsorption, due cognisance being taken of the higher temperature at which these experiments were conducted. An activation energy of adsorption of 38 kJ mol^{-1} (heat of adsorption of 35 kJ mol^{-1}) gave a hydrogen atom coverage of 33% of a monolayer (H : Cu = 0.33) at 396 K. Lowering the energy barrier by 4 kJ mol^{-1}, i.e., increasing the heat of adsorption to 38 kJ mol^{-1}, increased the hydrogen atom coverage at 396 K to 49% of a monolayer. On this basis, the activation energy of 38 kJ mol^{-1} for hydrogen adsorption was consistent with the upper limit of measured hydrogen.

1.12. Non-activated carbonate formation on copper

The surface coverages listed in Table 5 clearly show that, at steady state, during the reverse shift reaction, part of the surface of the copper that is catalysing the reaction is covered with oxygen atoms to an extent that is dependent on the detailed kinetics of the adsorption of hydrogen. The adsorption of CO_2 onto this area of surface oxidised copper will produce a surface carbonate [29]. In temperature programmed desorption experiments, this carbonate species desorbs as CO_2 at a peak maximum temperature of 333 K. The desorption/decomposition activation energy, E_d, derived

from this by application of the Redhead equation [37] Eq. (4)

$$\frac{E_d}{RT_m} = \frac{A}{\beta} e^{-E_d/RT_m} \quad (4)$$

where E_d/J mol^{-1} is the desorption activation energy, T_m/K is the desorption peak maximum temperature, R/J mol^{-1} is the gas constant, A/s^{-1} is the desorption pre-exponential term which is given an assumed value of 10^{13} s^{-1} and β/K s^{-1}, the heating rate, is 92 kJ mol^{-1}. This was incorporated into the detailed kinetics of the forward and reverse shift reaction (reaction nos. 9–16, Table 4) by the inclusion of reaction no. 17.

Reaction no.	$\log_{10}$ (A/units)	E/J mol^{-1}	$\log_{10}$ (A/s^{-1})	E/J mol^{-1}
17	13	0000	13	92000
	13	$CO_2 + O_{(s)} \rightleftharpoons$		
	13	$CO_{2(a)}$		

Reaction 17 assumes that the formation of the carbonate species is non-activated.

The prediction obtained by including the non-activated formation of a surface carbonate species having a heat of formation of 92 kJ mol^{-1} was that, at steady state, the surface would be totally carbonated and that no reaction would proceed. This was an important conclusion; the non-activated adsorption of a carbonate species having a heat of adsorption of 92 kJ mol^{-1} would completely cover the surface, with the effect of poisoning its activity. It could act merely as a spectator. For this to not happen, either the adsorption of the CO_2 to form a carbonate must be activated or the carbonate species once formed must be removed by further reaction, i.e., by hydrogenation to methanol. A corollary of the latter is that methanol synthesis would always have to accompany the forward and reverse shift reactions.

1.13. Activated carbonate formation on copper

Recently, we have explored the consequences of the adsorption of CO_2 to form a surface carbonate being activated and have revealed a subtle interplay between the values of the activation energies for the adsorption of both H_2 and CO_2 [38].

Table 5 lists the overall activation energies for the reverse shift reaction predicted by varying the energy barriers to H_2 and CO_2 adsorption. The experimentally determined overall activation energy for the reverse shift reaction is ~60 kJ mol^{-1} [21]. A combination of energy barriers of H_2 adsorption in the range 25 to 50 kJ mol^{-1}, with an energy barrier to carbonate formation of 21 kJ mol^{-1}, would correspond with experiment.

The measured exit CO concentration at 473 K was ~0.1% from a feed of CO_2/H_2 (5% CO, 95% H_2). Table 6 shows that activation energy barriers to H_2 adsorption, of between 17 and 50 kJ mol^{-1}, and to carbonate formation, of between 21 and 63 kJ mol^{-1}, predict exit CO concentrations in accord with the experiment.

The predicted coverages of the surface by carbonate, obtained by varying the energy barriers to H_2 and CO_2 adsorption, are listed in Table 7. There is a sharp cut-off in predicted carbonate coverages for activation energies for carbonate formation, >20 kJ mol^{-1}, regardless of the energy barrier to hydrogen adsorption. This parameter, therefore, is the best measure of the relative values of these energy barriers.

2. Conclusions

The method of microkinetic analysis described here is a technique of immense power. It deconvolutes the overall reaction into its component elementary reactions and assigns Arrhenius parameters to the forward and reverse of these. (The equilibrium constants for each of these elementary reactions are, therefore, implicitly included.) By solution of these equations, it is capable of predicting the rate of the overall reaction, described by these elementary reactions, and rate constants, under any set of conditions of temperature, pressure and contact time.

So many parameters are involved that it is always possible to achieve a fit between prediction and experiment. This was not our purpose in applying the method. The methodology applied by us was to hold rigidly to given canonical forms of the kinetics determined by surface science techniques (either high coverage or low coverage) and to explore their predictive

Table 6
The exit concentrations/(% atmosphere) predicted by changing the activation energies for CO_2 and H_2 adsorption

Energy barrier to H_2 dissociative adsorption ($kJ\,mol^{-1}$)	Energy barrier to CO_2 adsorption forming adsorbed carbonate ($kJ\,mol^{-1}$)			
	0	21	42	63
0	0.003	0.048	0.057	0.058
8.4	0.006	0.063	0.074	0.074
16.8	0.006	0.088	0.100	0.100
25.0	0.006	0.096	0.104	0.104
33.5	0.006	0.098	0.105	0.105
41.8	0.006	0.099	0.105	0.105
50.2	0.006	0.099	0.106	0.106

Table 7
The surface coverages of the carbonate species (% monolayer) by changing both the activation energy to CO_2 adsorption (maintaining the desorption activation energy at $92\,kJ\,mol^{-1}$) and the activation energy to H_2 adsorption

Energy barrier to H_2 dissociative adsorption ($kJ\,mol^{-1}$)	Energy barrier to carbonate formation/$kJ\,mol^{-1}$			
	0	21	42	63
0	91.5	45.0	0.5	0.002
8.4	80.8	18.6	0.1	0.001
16.8	92.8	42.9	0.5	0.002
25.0	96.6	65.8	1.0	0.005
33.5	98.1	76.8	1.0	0.008
41.8	98.6	81.3	2.2	0.011
50.2	98.8	83.0	2.4	0.012

capability when extrapolated to temperatures and pressures used industrially. Where the prediction was inaccurate, it was informative. In ammonia synthesis, the method predicted that the dissociation of the molecular nitrogen precursor should be activated. Whereas this had been found by Scholten and co-workers for nitrogen adsorption on an alumina-supported iron catalyst [13], it had not been found for a doubly promoted ($K/Al_2O_3/Fe$) catalyst. It was, however, subsequently discovered by Fastrup by temperature programmed adsorption [20].

Recently, Fastrup has attempted to understand the causes for the particular line-shape observed for the temperature dependence of the nitrogen uptake obtained in temperature programmed adsorption by the use of microkinetic analysis [39]. An adequate replication of the experimental line shape could be obtained only if the values of both the heat of adsorption of nitrogen and its desorption activation energy were coverage dependent, as had been found by Scholten and co-workers [13], although an adequate fit was obtained using nitrogen atom adsorption/desorption energetics similar to the high coverage values of Scholten and co-workers, which had been used by us previously [2,9]. The inadequacy of the use of Langmunian isotherms was explicitly acknowledged in our first paper by confining the predictions to high pressure or low pressure canonical forms of potential energy surface [2].

Nevertheless, the debate as to the exact nature of the dynamics of nitrogen adsorption on iron remains. Recently, Alstrup and co-workers, using XPS to determine nitrogen atom coverages, measured the temperature dependence of the nitrogen initial sticking probability by exposing an Fe(111) surface to gas phase nitrogen in the pressure range 10^{-4}–500 Torr (1 Torr = 133 Pa) and in the temperature range 393–578 K [40]. They found that the initial dissociative chemisorption probability was independent of gas temperature, concluding that dissociative

adsorption was precursor state mediated [40]. This result appears to be in direct disagreement with those obtained by Rettner and Stein using molecular beam scattering [41]. At beam energies corresponding to normal thermal energies, the initial sticking probability was $\sim 10^{-6}$. However, on increasing the beam kinetic energy to $100\,kJ\,mol^{-1}$ the initial sticking probability increased by a factor of 10^4.

Rationalisation of this dichotemy has been sought by Mortensen and co-workers in density functional calculations [42]. These predict the existence of a new molecularly held nitrogen precursor state (the α' state) between the well-known molecularly precursor state held parallel to the iron surface (the α state) and the atomically held nitrogen (the β state) on the reaction co-ordinate. Access to this state can be accomplished by two routes: (i) one which involves no energy barrier, but a large entropic barrier; and (ii) a direct route to the α' state, which involves a high energy barrier. It is predicted that at normal ammonia synthesis conditions, the high entropic barrier will dominate [42]. However, this does not appear to explain Scholten and co-workers' observation of activated adsorption in the temperature range 300–530 K and the pressure range of 7 to 100 Torr [13], nor of Fastrup's temperature programmed adsorption observation of a temperature dependent uptake of nitrogen, with an onset temperature of 400 K.

When the microkinetic methodology used by us was applied to the shift reaction over copper, it predicted a value for the activation energy for hydrogen adsorption on copper, which was identical to that found experimentally. In addition, it has predicted a value of 25 kJ mol for the activation energy for CO_2 adsorption on partially oxidised copper to form a carbonate. Measurement of the temperature dependence of the carbonate coverage in CO_2/H_2 streams would be a unique method for the determination of the relative values of these barriers.

References

[1] S.F. Bush, P. Dyer, Proc. R. Soc. London A 351 (1976) 33.
[2] M. Bowker, I.B. Parker, K.C. Waugh, Appl. Catal. 14 (1985) 101.
[3] G. Ertl, in: J.R. Anderson, M. Boudart (Eds.), Catalysis, Science and Technology, vol. 4, Springer, Berlin, 1983, p. 273.
[4] G. Ertl, Catal. Rev. Sci. Eng. 21(2) (1980) 201.
[5] G. Ertl, S.B. Lee, M. Weiss, Surf. Sci. 114 (1982) 527.
[6] F. Bozso, G. Ertl, M. Grunze, M. Weiss, J. Catal. 49 (1977) 18.
[7] M. Grunze, F. Bozso, G. Ertl, M. Weiss, Appl. Surf. Sci. 1 (1978) 241.
[8] J.W. Geus, K.C. Waugh, in: J.R. Jennings (Ed.), Catalytic Ammonia Synthesis, Plenum Press, New York, 1991, p. 196.
[9] K.C. Waugh, in: R.W. Joyner, R.A. van Santen (Eds.), Elementary Reaction Steps in Heterogeneous Catalysis, Kluwer Academic Publishers, Dodrecht, 1993, p. 407.
[10] F. Bozso, G. Ertl, M. Grunze, M. Weiss, Appl. Surf. Sci. 1 (1977) 103.
[11] G. Ertl, private communication.
[12] H.D. Vandervell, K.C. Waugh, Chem. Phys. Lett. 171 (1990) 462.
[13] J.J.F. Scholten, P. Zweitering, J.A. Konvalinka, J.H. de Boer, Trans. Faraday Soc. 55 (1959) 2166.
[14] N.D. Spencer, R.C. Schoonmaker, G.A. Somorjai, J. Catal. 74 (1982) 129.
[15] P. Stoltze, J.K. Norskov, Phys. Rev. Lett. 55 (1985) 2502.
[16] M. Bowker, I.B. Parker, K.C. Waugh, Surf. Sci. 197 (1988) L223.
[17] G. Ertl, S.B. Lee, M. Weiss, Surf. Sci. 114 (1982) 515.
[18] A. Nielsen, An Investigation of Promoted Iron Catalysts for the Synthesis of Ammonia, 3rd ed., J. Gjellerups, Copenhagen, 1968, p. 51.
[19] I.B. Parker, K.C. Waugh, M. Bowker, J. Catal. 114 (1988) 457.
[20] B. Fastrup, Topic Catal. 1 (1994) 273.
[21] R.A. Hadden, H.D. Vandervell, K.C. Waugh, G. Webb, Proc. 9th Int. Congr. Catal. 4 (1989) 1835.
[22] K.C. Waugh, Chem. Eng. Sci. 51 (1996) 1533.
[23] E. Tserpe, K.C. Waugh, in: B. Delmon, J.T. Yates (Eds.), Studies in Surface Science and Catalysis, Elsevier, Amsterdam, 1997, p. 401.
[24] T. van Herwijen, W.A. de Jong, J. Catal. 63 (1980) 83.
[25] R.A. Hadden, H.D. Vandervell, K.C. Waugh, G. Webb, Catal. Lett. 1 (1988) 27.
[26] A.J. Elliott, R.A. Hadden, J. Tabatabaei, K.C. Waugh, F.W. Zemicael, J. Catal. 157 (1995) 153.
[27] E. Colbourn, R.A. Hadden, H.D. Vandervell, K.C. Waugh, G. Webb, J. Catal. 130 (1991) 514.
[28] B.E. Hayden, C.L.A. Lamont, Phys. Rev. Lett. 63 (1989) 1823.
[29] J.M. Campbell, C.T. Campbell, Surf. Sci. 259 (1991) 1.
[30] P.B. Rasmussen, P.M. Holmblad, H. Christofferson, P.A. Taylor, I. Chorkendorff, Surf. Sci. 287/288 (1993) 79.
[31] M.J. Sandoval, A.T. Bell, J. Catal. 144 (1991) 227.
[32] J. Tabatabaei, B.H. Sakakini, M. Watson, K.C. Waugh, Cat. Lett., in press.
[33] G.J. Millar, C.H. Rochester, K.C. Waugh, J. Mol. Phys. 76 (1991) 833.
[34] J. Nakamura, J.A. Rodriguez, C.T. Campbell, J. Phys. Condens. Matter 1 SB (1989) 149.
[35] A.J. Elliott, B.H. Sakakini, J. Tabatabaei, K.C. Waugh, in preparation.

[36] M. Muhler, L.P. Nielson, E. Tornqvist, B.S. Clausen, H. Topsoe, Catal. Lett. 14 (1992) 241.
[37] P.A. Redhead, Trans. Faraday Soc. 57 (1961) 641.
[38] L. Watremetz, M.Sc. Diss., UMIST, Manchester, 1997, p. 46.
[39] B. Fastrup, J. Catal. 168 (1997) 235.
[40] I. Alstrup, I. Chorkendorff, S. Ullmann, J. Catal. 168 (1997) 217.
[41] C.T. Rettner, H. Stein, Phys. Rev. Lett. 59 (1987) 2768.
[42] J.J. Mortensen, L.B. Hansen, B. Hammer, J.K. Norskov, J. Catal. 182 (1999) 479.